# Evaluation of Photocatalysts for Water Splitting through Combined Analysis of Surface Coverage and Energy-Level Alignment

Zhendong Guo[a],* Francesco Ambrosio[b] and Alfredo Pasquarello

*Chaire de Simulation à l'Echelle Atomique (CSEA), Ecole Polytechnique Fédérale de Lausanne (EPFL), CH-1015 Lausanne, Switzerland*

E-mail: zdguo@suda.edu.cn

[a]Present address: College of Energy, Soochow Institute for Energy and Materials InnovationS (SIEMIS), Soochow University, Suzhou 215006, China

[b]Present address: 1. Computational Laboratory for Hybrid/Organic Photovoltaics (CLHYO), Istituto CNR di Scienze e Tecnologie Molecolari (ISTM-CNR), Via Elce di Sotto 8, 06123 Perugia, Italy
2. CompuNet, Istituto Italiano di Tecnologia, Via Morego 30, 16163 Genova, Italy

**Abstract**

To examine whether suitable conditions occur for the water splitting reaction at their interfaces with liquid water, we determine the pH-dependent surface coverage for a series of semiconductors, including GaAs, GaP, GaN, CdS, ZnO, $SnO_2$, rutile and anatase $TiO_2$. For this we calculate acidity constants at surface sites through *ab initio* molecular dynamics simulations and a grand-canonical formulation of adsorbates. The resulting pH values at the point of zero charge show excellent agreement with experiment and thereby support the validity of our approach. By combining information concerning the surface coverage with the alignment of the band edges with respect to the relevant redox levels, we scrutinize the potential of the considered semiconductors as photocatalysts and identify the corresponding optimal pH ranges for hydrogen and oxygen evolution. More specifically, our results indicate that GaN stands out among

these semiconductors as the most promising candidate for the overall water splitting, with the potential of further improvement through alloying. With the surface coverage, our computational analysis brings a new descriptor that is at present beyond experimental reach.

Keywords: water splitting, semiconductor-water interface, acidity constant, surface coverage, band alignment, thermodynamic integration, molecular dynamics simulation

# Introduction

Despite the extensive attention from the scientific community[1–10] and the tremendous efforts devoted,[11–17] the efficiency of heterogeneous photocatalytic water splitting is still by and large unsatisfactory.[1,18] This precludes any large-scale commercial application of this otherwise promising technology for the production of clean fuel.[18] One of the key features currently hindering any perspective use of this process is the lack of an efficient photocatalyst material.[19]

In principle, any semiconductor that is stable in aqueous environment and capable of harvesting solar light could be a photocatalyst for the water splitting reaction, thus providing a plethora of candidate materials. This enormous set might be reduced by considering several supplementary requirements for the ideal catalyst, such as a favorable alignment of the band edges with respect to the redox levels of liquid water,[20] a long lifetime and high mobility of the charge carriers,[21–23] a high resistance to corrosion, a strong defect tolerance, and a large ensuing photovoltage.[24] Another factor that is equally important but that has received less attention, is the propensity to dissociate water molecules upon surface absorption.[25,26] The spontaneous occurrence of dissociated water molecules in the form of ionic species like $H^+$ and $OH^-$ in near-neutral conditions is certainly beneficial for promoting hydrogen or oxygen evolution,[27] and allows one to avoid extremely acidic or alkaline solutions, which could more easily induce electrode degradation. However, in practice, all these properties cannot be

tested experimentally for so many candidate materials.

Therefore, since the first investigations of heterogeneous water splitting,[11] computational chemistry and physics have been used to disentangle some of the phenomena that are relevant to the efficiency of this process and to introduce an element of design in the systematic exploration of candidate materials.[19,25,26,28–44] Because of the recent development of advanced electronic-structure methods, excellent results have been achieved in the calculation of the band gap of semiconductors[45–49] as well as in the alignment of the band edges at water-semiconductor interfaces.[20,25,28,37] Based on simplified computational protocols, theoretical screenings of candidate materials have been deployed[19,30–33] in order to define smaller sets of possibly promising photocatalysts with appropriate band gaps and band edges favorably aligned to the redox levels of hydrogen reduction and water oxidation.[20] Furthermore, the calculation of the overpotentials associated to the water oxidation reaction has been made possible both by means of simplified interface models[29,41,50–53] and, more recently, by means of more realistic semiconductor-water interfaces in a few cases.[41,54]

In this framework, the theoretical description of physical processes occurring at semiconductor-water interfaces is complicated by their multi-faceted nature, which depends upon various factors, e.g. the pH of the aqueous solution in which the material is immersed and possible reconstructions and defects at the surface.[26,35] Therefore, simplified computational protocols in which such effects are completely ignored, are likely to miss important physical aspects, thus affecting and possibly invalidating the achieved results. While the simultaneous inclusion of all effects in a single simulation remains currently beyond reach, it has recently been shown that theoretical approaches are at least capable of describing the acid-base chemistry and reactivity of pristine semiconductor-water interfaces.[25,26] However, in order to identify the characteristics of the ideal photocatalyst, it is necessary to enable a more extensive screening, in which semiconductor-water interfaces are modeled at the atomistic level and additional criteria besides band gaps and band edge positions are considered.

We here study the acid-base chemistry and reactivity of eight different semiconductors at

the interface with liquid water: GaAs(110), GaP(110), GaN($10\bar{1}0$), CdS($10\bar{1}0$), ZnO($10\bar{1}0$), $SnO_2$(110), rutile $TiO_2$(110) (r-$TiO_2$), and anatase $TiO_2$(101) (a-$TiO_2$), building upon previously determined interfacial structures and band alignments at these semiconductor-water interfaces.[28] By combining extensive *ab initio* molecular dynamics (MD) simulations with a grand-canonical formulation of adsorbates at the semiconductor water interface,[26,55] we determine the pH at the point of zero charge ($pH_{PZC}$) and find excellent agreement with the available experimental characterization[28] for all considered semiconductors. Through calculating the acidic constant ($pK_a$) of the individual adsorption sites at the interface, we are capable of investigating for each material the stability of adsorbed protons, hydroxyl ions, and water molecules at different values of pH. Furthermore, we align the band edges of the considered semiconductors at the interface with water by applying a scheme based on the line-up of the potential and on a computational standard hydrogen electrode.[25,28,56] By combining the acid-base chemistry with the alignment of the band edges with respect to the redox levels pertaining to the water splitting reaction, we examine the potential of the investigated semiconductors to act as efficient photocatalysts and identify the optimal pH ranges of operation for hydrogen and oxygen evolution. Among the considered materials, our approach identifies GaN as the most promising photocatalyst for achieving overall water splitting in near-neutral conditions and indicates the possibility of achieving further improvement through alloying.

# Methods

In this work, we determine site-specific acidity constants $pK_a$ at semiconductor-water interfaces within a grand-canonical formulation of adsorbates.[26,55] The formulation has been generalized to include molecular, dissociative and mixed adsorption modes, as described in sec. S1 of the Supplementary Information (SI). In this method, deprotonation free energies of adsorbed protons and water molecules are calculated through the thermodynamic integra-

tion method (see sec. S3 of the SI), which involves both molecular dynamics simulations of neutral interfaces as well as of interfaces with charged adsorbates (see sec. S2 of the SI). As far as the neutral interfaces are concerned, we take advantage of previously generated molecular dynamics trajectories for equilibrated semiconductor-water interfaces[28] and calculate the relevant energy differences upon deprotonation. The molecular dynamics simulations of the charged species are run on purpose in the present study and then used for the calculation of the thermodynamic integrals.

The molecular dynamics simulations used in this work are performed with a semilocal functional, which accounts for nonlocal van der Waals interactions (r-VV10).[57,58] The parameter $b$ of the rVV10 functional is set to the value of 9.3, in order to correctly reproduce the density and the structural properties of liquid water.[59] All the relevant energy differences associated to the molecular dynamics trajectories are first obtained consistently within the same semilocal scheme. Then, the deprotonation energies corresponding to the same structural configurations are also evaluated at the hybrid functional level. For this, we use the hybrid functional h-rVV10, which combines the PBE0 hybrid functional with the rVV10 description of nonlocal van der Waals interactions.[60] In this hybrid functional, the fraction $\alpha$ of Fock exchange is set to 0.40 and the $b$ parameter of rVV10 to 5.3, as these parameters have been found to give a good description of the density and the structural properties of liquid water.[60] Accordingly, the values of $\mathrm{pH_{PZC}}$ and the acidity constants ($\mathrm{p}K_\mathrm{a}$) at the studied semiconductor-water interfaces are determined at both levels of theory (see sec. S4 of the SI). Our results show that the hybrid functional yields $\mathrm{pH_{PZC}}$ in much better agreement with experiment than the semilocal functional. Notably, the $\mathrm{p}K_\mathrm{a}$ are found to be even more sensitive to the adopted level of theory, with the semilocal functional significantly overestimating the $\mathrm{p}K_\mathrm{a}$ of protons adsorbed on specific non-metal surface sites, such as As, P, and S (see sec. S4 of the SI). Consequently, the presentation in the following focuses on the results obtained at the hybrid functional level and the reader is referred to sec. S4 of the SI for a discussion of the semilocal results. A more extensive description of the applied methodologies is given

in sec. S3 of the SI.

## Results and Discussions

The values of $pH_{PZC}$ obtained at the hybrid-functional level are reported in Fig. 1(a) for comparison with experimental estimates.[28] The agreement with the measured values is excellent as demonstrated by the mean average error (MAE) of only 0.75 pH unit (see sec. S4 of the SI). This corresponds to an energy error lower than 0.05 eV, well within the typical accuracy of the hybrid-functional methods applied here (0.1–0.2 eV). In particular, for GaAs, GaP, and a-$TiO_2$, the calculations have been carried out using two different adsorption modes at the interface: (i) a molecular ($m$) mode in which water molecules are adsorbed on the metal sites M (e.g. Ga and Ti atoms) and (ii) a dissociative ($d$) mode in which hydroxyl ions are adsorbed on the metal sites M while protons are attached to the non-metal sites A (e.g. As, P, and O atoms). The consideration of two interface models for these semiconductors is motivated by the fact that both the $d$ or $m$ modes appear to be stable on the time-scales of our MD simulations, while this is not necessary for the other semiconductors for which the MD runs show a rapid conversion to a unique type of adsorption mode irrespective of the starting configuration.[28] Nevertheless, it is reassuring to find that the $pH_{PZC}$ calculated with $m$ and $d$ models differ negligibly (i.e. by less than 0.6 pH units, see sec. S4 of the SI).

The remarkable accuracy achieved for the values of $pH_{PZC}$ enables us to further analyze the acid-base chemistry of the water-semiconductor interfaces under consideration. In particular, we investigate the acidic constants of adsorbed protons on the non-metal sites A [$pK_a(H_A^+)$] and of adsorbed water molecules on the metal sites M [$pK_a(w_M)$] for each semiconductor surface. The respective acidic constants from our calculations are illustrated in Figs. 1(b) and (c), where they are compared with the acidic constant of the aqueous hydronium cation [$pK_a(H_3O^+)=-1.74$, by definition] and with that of an aqueous water molecule [$pK_a(H_2O)=15.74$], respectively. For all the interfaces, we find that the acidity of the ad-

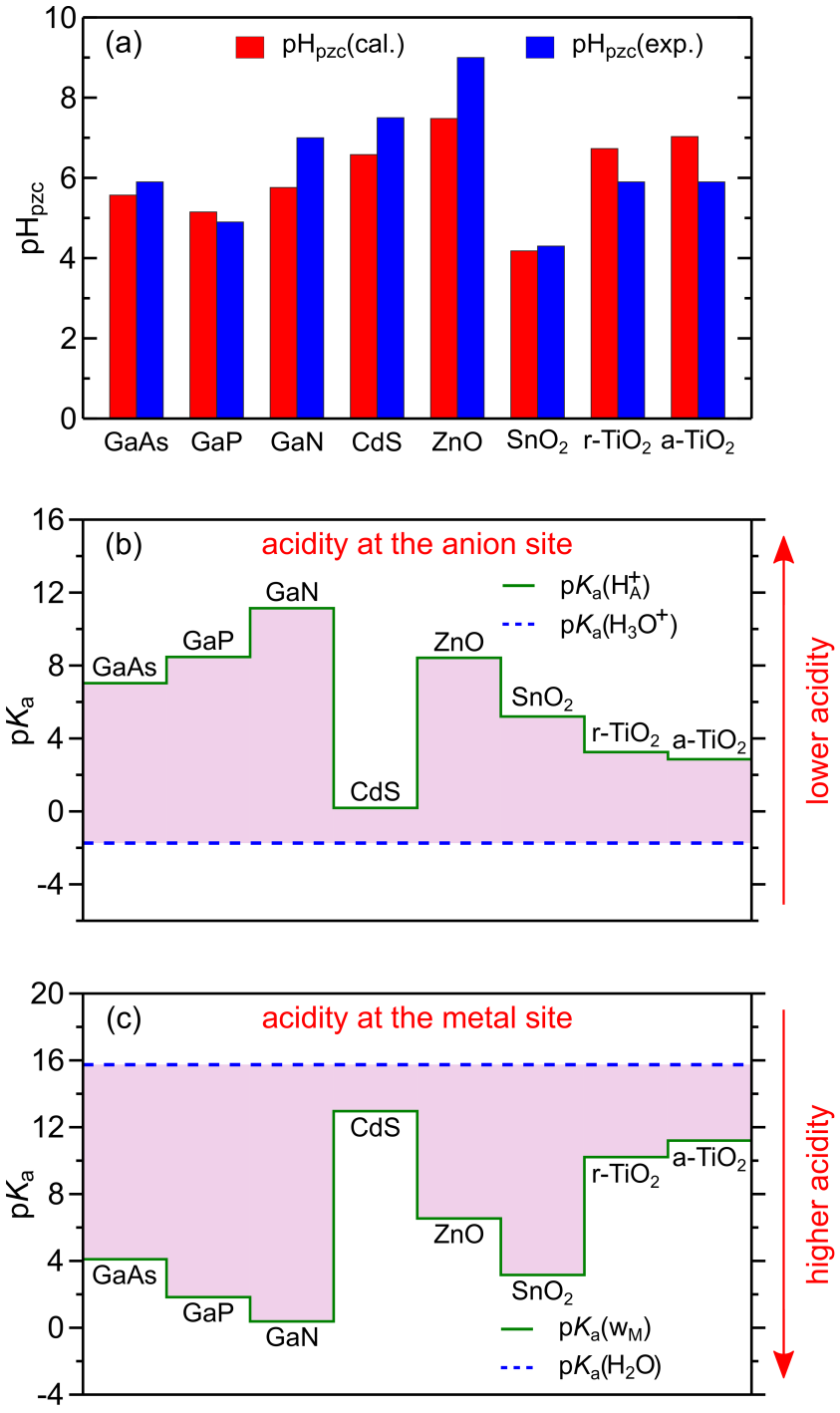


Figure 1: (a) Calculated values of $\mathrm{pH_{PZC}}$ (red bars) at various semiconductor-water interfaces compared with experimental estimates taken from Ref. 28 (blue bars). (b) p$K_\mathrm{a}$ of the proton ($\mathrm{H_A^+}$) adsorbed on a non-metal site A of the surface (e.g. As, P, N, S, and O atoms). (c) p$K_\mathrm{a}$ for the water molecule ($\mathrm{w_M}$) adsorbed on a metal site M of the surface (e.g. Ga, Cd, Zn, Sn and Ti atoms). In panel (b) and (c), the blue dashed lines indicate the p$K_\mathrm{a}$ for aqueous hydronium ions and water molecules, respectively. All values are reported in units of pH.

sorbed proton is noticeably weaker than that of the aqueous hydronium cation. However, we can distinguish two different behaviors. Oxides and sulfides, with the exception of ZnO, show a moderately acidic adsorbed proton. In particular, a value of $pK_a(H_A^+)$ as low as 0.19 is obtained for CdS. Anatase and rutile show similar properties with values of $pK_a(H_A^+)$ close to 3, while a higher alkalinity is observed for $SnO_2$ [$pK_a(H_A^+)$=5.20] and, more remarkably, for ZnO [$pK_a(H_A^+)$=8.42]. At variance, the non-metal sites A of the III-V semiconductors are rather alkaline with values of $pK_a(H_A^+)$ up to 11.14 for GaN. It is interesting to point out that, comparing GaN, GaP, and GaAs, we observe an increasing acidity of the proton site going from N to As, in agreement with the decreasing electronegativity.

In Fig. 1(c), the $pK_a(w_M)$ pertaining to the metal sites of the various semiconductors are compared with the corresponding acidic constant of the aqueous water molecule calculated at the same level of theory. III-V semiconductors show the largest differences with $pK_a(w_M)$ values ranging between 0.38 for GaN and 4.10 for GaAs. Since the water molecules are always adsorbed on a Ga surface site in these cases, it is evident that also the surrounding chemical environment, as determined by the nearest neighbors and the surface structure (110 for GaAs and GaP, $10\bar{1}0$ for GaN), affect the acidity of the adsorbed water molecules. For oxides and sulfides, we observe alkaline values of $pK_a(w_M)$ for CdS and for the two polymorphs of $TiO_2$. By contrast, the acidity of adsorbed water molecules is noticeably increased for ZnO [$pK_a(w_M)$=6.54], and even more so for $SnO_2$ [$pK_a(w_M)$=3.16].

Overall, the calculated data should be interpreted taking into account the different electronegativities of the surface sites but also the chemical environment at the surface. For example, while CdS and ZnO have a very similar surface structure, the calculated values of both $pK_a(H_A^+)$ and $pK_a(w_M)$ are completely different, because of the intrinsic difference in reactivity of the surface sites. Similarly, we observe that surface O sites of different semiconductor surfaces can span a large range of values for $pK_a(H_A^+)$. Hence, a clear role should be assigned to the chemical environment at the surface in modulating the acidity of chemically equivalent sites. It is important to underline that the complex interplay between intrinsic

reactivity and chemical environment might not be captured by simplified models.

By combining the results achieved for $\mathrm{p}K_\mathrm{a}(\mathrm{H_A^+})$ and $\mathrm{p}K_\mathrm{a}(\mathrm{w_M})$, it is also possible to determine the natural tendency of a given semiconductor surface to induce water dissociation. This is done by defining the free energy of dissociation for adsorbed water molecules ($\Delta A_\mathrm{d}$):[26,61]

$$\Delta A_\mathrm{d} = \ln 10 \cdot k_\mathrm{B} T [\mathrm{p}K_\mathrm{a}(\mathrm{w_M}) - \mathrm{p}K_\mathrm{a}(\mathrm{H_A^+})], \tag{1}$$

where $k_\mathrm{B}$ is the Boltzmann constant and $T$ the temperature. Negative values of $\Delta A_\mathrm{d}$ indicate exothermic dissociation of the adsorbed water molecules, while positive values make the process unfavorable, thus favoring adsorption of molecular water. We remark that through the calculation of $\Delta A_\mathrm{d}$ the thermodynamic integration method allows one to identify the most stable adsorption mode, even when regular molecular dynamics fail to overcome the energy barriers separating different surface configurations.[28] In Fig. 2, we illustrate the calculated values of $\Delta A_\mathrm{d}$ for the eight studied semiconductors. Again, we can broadly distinguish two groups of semiconductors. III-V semiconductors favor the dissociation of the $H_2O$ molecules with a clear trend towards more favorable dissociation as the electronegativity of the anion increases along the series GaAs, GaP, and GaN. At variance, oxides and sulfides appear to favor molecular adsorption of water molecules on their pristine surfaces, with the exception of $SnO_2$ and ZnO, which show moderately negative values for $\Delta A_\mathrm{d}$ ($\sim -0.15$ eV). This result is consistent with the outcome of molecular dynamics simulations for these two interfaces,[28] for which the coexistence of molecular and dissociated water molecules is observed. For both a-$TiO_2$ and r-$TiO_2$, we find $\Delta A_\mathrm{d}$ of $\sim$0.5 eV, indicating that the water molecules are molecularly adsorbed on their pristine surfaces. The present method thus provides an unequivocal description of the surface adsorption mode, improving upon straightforward molecular dynamics simulations, which were unable to sort out the issue in the case of a-$TiO_2$(101).[28] In addition, we note that the calculated energetic preference is remarkably higher than the experimentally measured energy difference of 0.035 eV between a molecularly and a dissociatively adsorbed water molecule on the r-$TiO_2$(110) surface exposed to the

vacuum.[62] This discrepancy should be attributed to the solvent which stabilizes the adsorbed water molecules in the simulations.

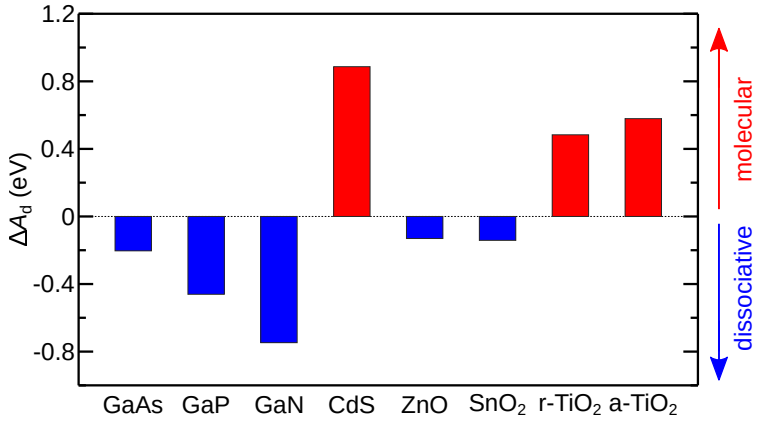


Figure 2: Calculated free energy of dissociation for adsorbed water molecules on various semiconductor surfaces. Red (blue) bars indicate that the molecular (dissociative) adsorption mode is favored.

The calculated acidity constants do not only provide insight into the physico-chemical properties of the semiconductor-water interfaces, but they also allow for a detailed description of the pH-dependent surface chemistry of such interfaces. This is achieved by constructing logarithmic diagrams of concentration, commonly employed for weak acids in aqueous solution, and recently extended to semiconductor-water interfaces.[26] In Fig. 3, we illustrate this powerful instrument for visualizing the acid-base properties of the interfaces studied. However, it should be realized that inaccuracies of about 1-2 pH units for $\mathrm{p}K_{\mathrm{a}}(\mathrm{H}_{\mathrm{A}}^{+})$ and $\mathrm{p}K_{\mathrm{a}}(\mathrm{w}_{\mathrm{M}})$ may lead to sizeable variations of equilibrium concentrations due to the exponential dependence of such concentrations on energy (see sec. S1 of the SI). The concentration diagrams for GaAs, GaP, and GaN are rather similar, all showing a preference for dissociative water adsorption at $\mathrm{pH}_{\mathrm{PZC}}$. In the case of GaAs(110) [Fig. 3(a)], the ratio between the concentrations of dissociatively and molecularly adsorbed water at $\mathrm{pH}_{\mathrm{PZC}}$ is found to be close to 30:1, implying that only $\sim 3\%$ of the adsorbed water retains its molecular form. This is consistent with in-situ near-ambient pressure XPS studies revealing dissociative adsorption of water at the GaAs-water interface.[63] For GaP(110) [Fig. 3(b)] and GaN($10\bar{1}0$) [Fig. 3(c)], the concentration of ionic species exceeds that of molecular adsorption by over

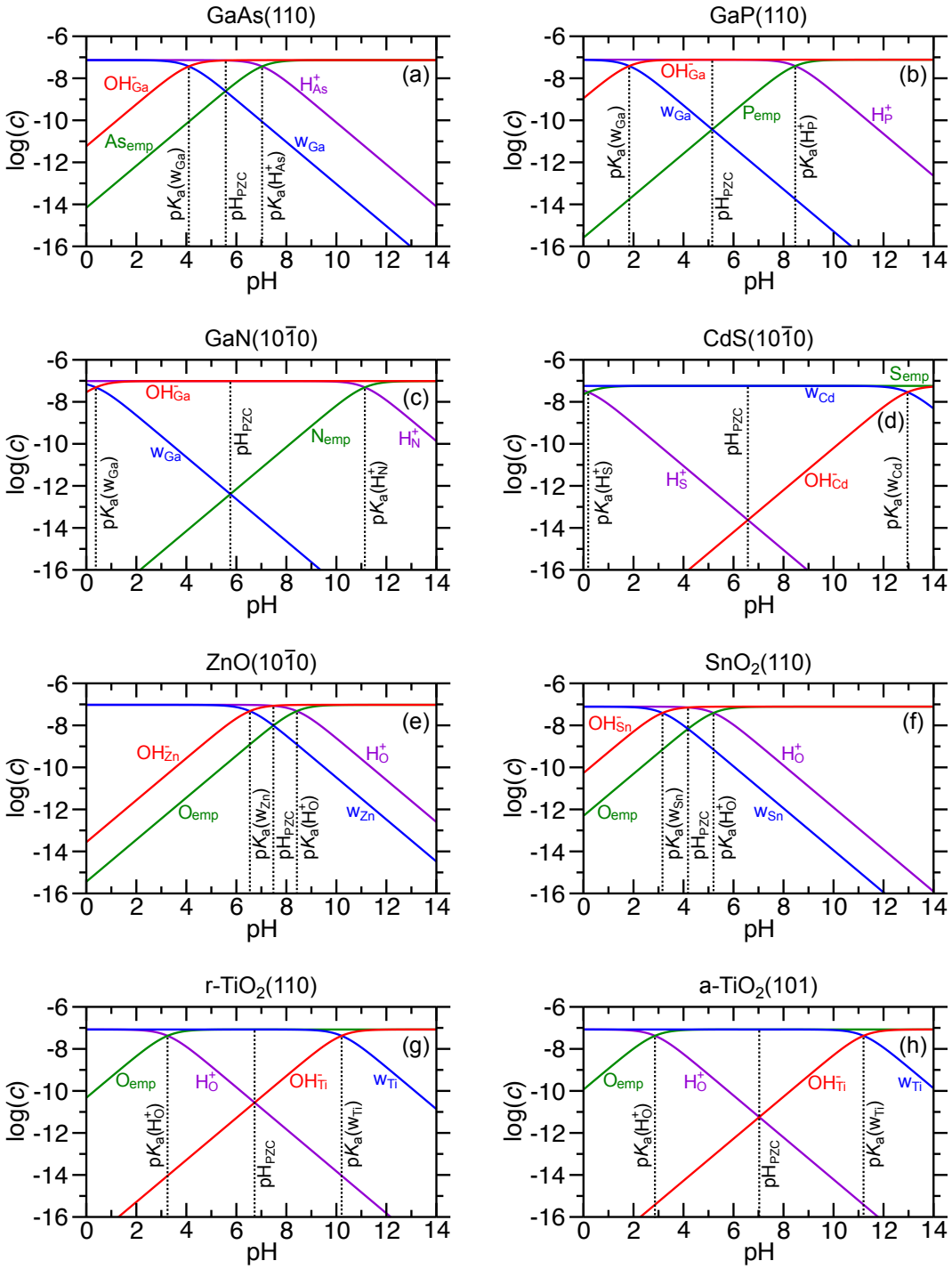


Figure 3: Acid-base logarithmic diagrams for the coverage of pristine (a) GaAs(110), (b) GaP(110), (c) GaN(10$\bar{1}$0), (d) CdS(10$\bar{1}$0), (e) ZnO(10$\bar{1}$0), (f) $SnO_2$(110), (g) r-$TiO_2$(110) and (h) a-$TiO_2$ (101) surfaces in aqueous environment, as calculated at the h-rVV10 level of theory. The concentration values $c$ are expressed in mol/dm$^2$.

three orders of magnitude at $pH_{PZC}$, indicating that the model showing complete dissociation is representative of the real interface.[28] In near-neutral conditions, at which an ideal water-splitting plant should operate,[1] almost 100% of the surface Ga sites are passivated by hydroxyl ions for these Ga-based semiconductors. Hence, the water oxidation reaction on these surfaces will proceed through the reaction mechanism occurring under alkaline conditions (i.e. through the oxidation of the adsorbed hydroxyl ions),[27] which is kinetically more favorable and faster than the reaction mechanism occurring under acidic conditions (i.e. the dehydrogenation of the adsorbed water molecules).[27] At pH $\cong$ 7, we find roughly 52% of the surface As sites to be protonated, while the respective percentages increase to $\sim$ 97% and 100% for surface P and N sites. In the case of GaAs, we observe a rather narrow pH window ($4.1 < pH < 7.0$), within which protons and hydroxyl ions are the dominant adsorbed species. The corresponding pH windows are wider for GaP and GaN, where they extend from 1.8 to 8.5 and from 0.4 to 11.1, respectively. These large pH windows are particularly desirable for the overall photocatalytic water splitting reaction, for which adsorption of both ionic species is realized without enforcing extremely acidic (for protons) or alkaline (for hydroxyl ions) conditions. For pH values lower than 4.1 for GaAs, 1.8 for GaP and 0.4 for GaN, molecular water becomes the dominant adsorbate and the water oxidation reaction would then mainly proceed through the dehydrogenation of adsorbed water molecules, for which the mechanism is slow and kinetically unfavorable. This explains why the water-splitting efficiency at a GaN photoanode is poorer in the presence of electrolytes like $H_2SO_4$ than like KOH or NaOH.[64]

The diagrams for ZnO [Fig. 3(e)] and $SnO_2$ [Fig. 3(f)] highlight their peculiar surface coverage, by which protons and hydroxyl ions simultaneously dominate the adsorbed species only in a rather narrow pH range ($6.5 < pH < 8.4$ for ZnO and $3.2 < pH < 5.2$ for $SnO_2$). For these materials, we observe at $pH_{PZC}$ the coexistence of ionic species, unoccupied surface O sites, and molecularly adsorbed water, consistent with previous MD simulations indicating the occurrence of a mixed adsorption mode.[28] At pH $\cong$ 7, the surface coverages of ZnO and

$SnO_2$ differ noticeably. For ZnO, nearly three out of four surface Zn sites are passivated by hydroxyl ions and the percentage of protonated surface O sites is as high as 96%, showing favorable conditions for the overall water splitting reaction. Instead, such conditions are less convenient for $SnO_2$. Although all surface Sn sites are also favorably covered by hydroxyl groups, the fraction of adsorbed protons becomes negligible. This adsorption mode in near-neutral conditions supports $SnO_2$ as a good photocatalyst for oxygen evolution rather than for the overall water splitting reaction. For making $SnO_2$ more suitable for the latter reaction, it would be preferable to operate in slightly acidic conditions (e.g. at pH $\cong$ 4).

The situation is completely different in the case of CdS [Fig. 3(d)], for which the concentrations of ionic adsorbates at $pH_{PZC}$ are $\sim$ 6 orders of magnitude lower than that of molecularly adsorbed water. This result is fully consistent with the outcome of previous MD simulations, where it has been found that the molecular adsorption mode is spontaneously realized.[28] We notice that the fraction of adsorbed protons and hydroxyl ions is negligible over a pH interval ranging from 1 to 12. Therefore, CdS would operate as a poor photocatalyst for the overall water splitting reaction, as the reduction of protons on its surface is largely adsorption limited. To achieve overall water splitting, one should operate in extremely acidic conditions (pH $<$ 1) where adsorbed protons begin to appear, but even in this case water oxidation would proceed through the slow and kinetically unfavorable mechanism involving adsorbed water molecules. Only when pH $>$ 13, the surface is prevalently hydroxylated and the oxidation could proceed through the more favorable mechanism involving the adsorbed hydroxyl ions. Hence, the present analysis indicates that CdS is not a suitable photocatalyst for either the hydrogen reduction or the water oxidation reaction.

The concentration diagrams for the two phases of $TiO_2$ [Fig. 3(g) and (h)] are similar to that of CdS, with molecular adsorption dominating over a large pH range (3.3 $<$ pH $<$ 10.2 for r-$TiO_2$ and 2.9 $<$ pH $<$ 11.2 for a-$TiO_2$). At $pH_{PZC}$, the concentrations of ionic species are at least 4 orders of magnitude lower than that of molecularly adsorbed water. $H^+$ and $OH^-$ ions are found in significative concentrations only at acidic and alkaline conditions, re-

spectively. Such conditions are not convenient for the operation of an overall water splitting device. At near-neutral pH, the hydrogen evolution would be hindered by the absence of adsorbed protons and the oxygen evolution reaction would occur through the slow mechanism associated with the dehydrogenation of water molecules,[27] while the kinetically more favorable mechanism involving oxidation of adsorbed hydroxyl ions[27] would be inhibited. The latter tendency could be reversed only at highly alkaline values of pH, where one would, however, face the issue of surface degradation. This result is consistent with the experimental observation that rutile $TiO_2$ powder shows low activity for the overall water splitting at pH = 2, due to the extremely low rate of oxygen evolution.[65] Furthermore, it has experimentally been found that r-$TiO_2$ yields the highest photocatalytic performance at pH = 5.5.[65] This observation can be understood as follows. From Fig. 3(g), we notice that the pH of 5.5 corresponds to the highest value at which some of the O sites at the surface (about 1%) are still protonated. In this acidic condition, hydroxyl groups do not occur on pristine r-$TiO_2$(110) according to our calculations, but such adsorbates could be stabilized by the occurrence of defects at the surface, such as oxygen vacancies, which significantly promote the dissociation of adsorbed water molecules.[66] The optimal pH value then results from a trade off. For more alkaline solutions the hydrogen evolution is inhibited due to the lack of adsorbed $H^+$, whereas the defect-induced $OH^-$ ions would suffer from the recombination with protons in more acidic conditions, leading in turn to the poor efficiency of $O_2$ evolution.

The adsorption of suitable reactants is surely a precondition for heterogeneous photocatalytic water splitting, but is not sufficient to ensure the efficiency of the process. In fact, a desirable acid-base chemistry of the semiconductor-water interface must also rely on a favorable alignment between the electrochemical energy levels involved in the proton-coupled electron transfer reactions,[50] namely the band edges of the semiconductors, which provide the charge carriers, and the redox potentials associated with hydrogen reduction and water oxidation. By combining the band alignment at the semiconductor-water interface with the description of the surface chemistry, one can infer whether the photocatalytic reactions

run efficiently.[25] Hence, for each semiconductor, we consider an energy level diagram that includes the band edges and the relevant redox levels (cf. Fig. 4). We take the band edges as calculated in Ref. 28 and revised according to the improved estimate of the SHE level proposed in Ref. 67. We here use calculated band edges rather than experimental ones to demonstrate that our theoretical approach is self-standing, but the use of experimentally determined band edges in Fig. 4 would not affect any of the relative energy positions.

Since the hydrogen evolution reaction is generally not responsible for slowing down the overall water splitting reaction,[50] we do not explicitly consider intermediate states associated to surface adsorption and directly focus on the $H^+/H_2$ redox level in solution, which corresponds to the SHE at pH = 0. At variance, in the case of the oxygen evolution reaction, intermediate states adsorbed at the surface are known to play a more critical role leading to significant overpotentials.[50] Hence, we focus on the $OH^-/OH^\bullet$ redox level for the oxidation

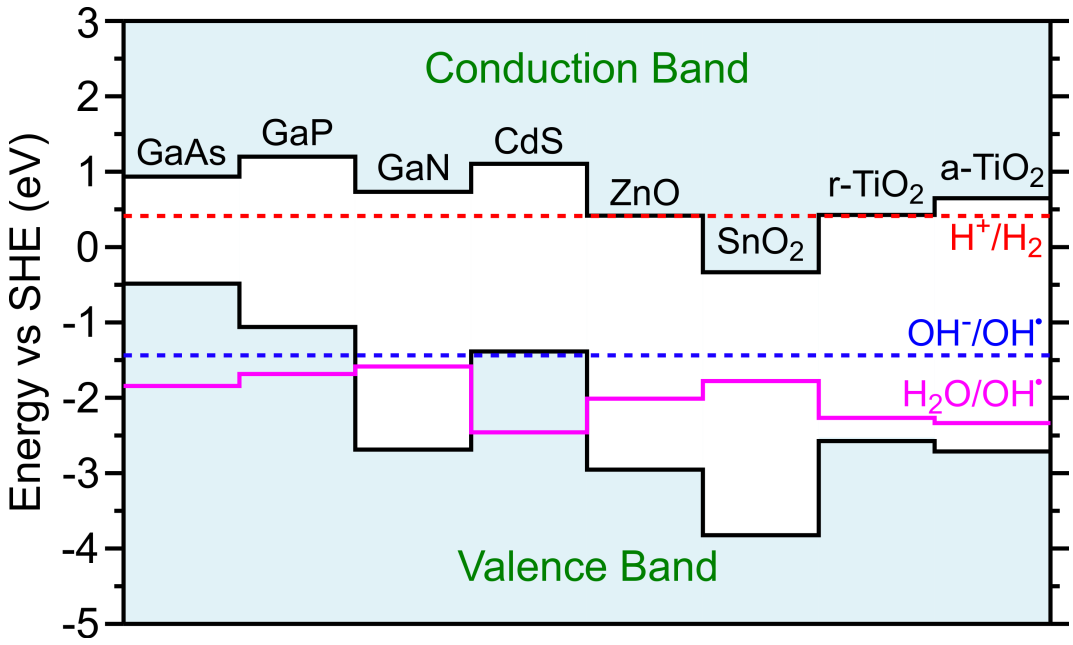


Figure 4: Band edges together with relevant redox levels ($H^+/H_2$ in dashed red, $OH^-/OH^\bullet$ in dashed blue, and $H_2O/OH^\bullet$ in solid magenta) at various semiconductor-water interfaces at pH=7, referred to the SHE. We take band edges as calculated at the PBE0($\alpha$) level in Ref. 28 and revised according to the improved estimate of the SHE level reported in Ref. 67. The redox levels $H^+/H_2$ and $OH^-/OH^\bullet$ have been calculated in the solution (see sec. S1 of the SI) and are taken from Ref. 56.

of adsorbed hydroxyl anions and on the $H_2O/OH^\bullet$ redox level for the dehydrogenation of adsorbed water molecules, which represent the first step of the water oxidation process in alkaline and acidic conditions, respectively.[27] The associated overpotentials result from the oxygen oxidation chemistry, but generally also depend on the specific material under consideration. For the adsorbed hydroxyl anions at $pH_{PZC}$, we account for the oxygen oxidation chemistry by taking as indicative redox level the one pertaining to the aqueous hydroxyl ion,[56] but disregard material-specific differences in the same spirit as for the hydrogen evolution reaction. In the case of r-TiO2(110), the oxidation potentials of the $OH^-/OH^\bullet$ level calculated in liquid water[56] and at the solvated interface[41,68] differ by less than 0.05 eV, supporting this way of proceeding. We infer the $H_2O/OH^\bullet$ redox level from a two-step process involving sequentially the deprotonation of the adsorbed water molecule and the oxidation of the hydroxyl ion. Furthermore, we assume ideal conditions in which the band edges of the semiconductors and the relevant redox levels follow a Nernstian behaviour, i.e. they move closer to the vacuum level with increasing pH at the rate of 0.059 eV per pH unit. In particular, it is important to remark that the relative positions between the band edges of the semiconductors and the redox levels do not depend on pH. For a more detailed discussion of the redox levels, we refer the reader to sec. S1 of the SI.

As can be seen in Fig. 4, the conduction band edges of all the semiconductors studied are favorably aligned with respect to the $H^+/H_2$ redox level with the sole exception of $SnO_2$, suggesting that these materials are suitable for photocatalytic hydrogen evolution. For the oxidation of water, the valence band edges of GaAs, GaP, and CdS are significantly higher than the redox levels of $OH^-/OH^\bullet$ and $H_2O/OH^\bullet$, making of these materials poor photocatalysts. The valence band edges of the other semiconductors lie at least 0.3 eV lower than the $OH^-/OH^\bullet$ and $H_2O/OH^\bullet$ levels, implying that these materials are suitable for photocatalytic water oxidation.

For evaluation, we provide in Fig. 5 a global overview of the photocatalytic potential of the investigated semiconductors by combining information concerning the surface coverage

and the energy level alignment. Considering that highly acidic or alkaline solutions generally degrade the water splitting devices, we focus our attention onto those semiconductors that show significant coverage with ionic adsorbates and favorable alignment in near-neutral conditions ($5 \leq \mathrm{pH} \leq 9$). Hence, in Fig. 5, the occurrence of blue bars for the ionic adsorbates ($H^+$ and $OH^-$) within the yellow stripe signals the possibility of efficient hydrogen and oxygen evolution in the most favorable pH range. In this way, we infer that the Ga-based compounds and ZnO are the most suitable photocatalysts for hydrogen reduction, while water oxidation is best achieved with $SnO_2$, ZnO, and GaN. Among these semiconductors, GaN is the most promising candidate for the all-in-one reaction showing the largest range of suitable pH values. ZnO stands out as an alternative candidate with a band alignment

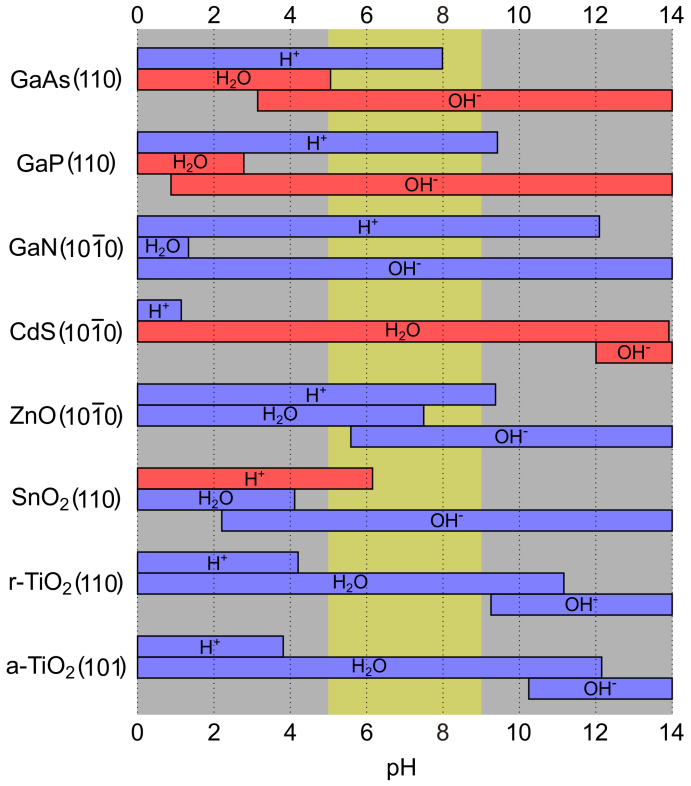


Figure 5: Combined view on the surface coverage and alignment for the various semiconductors. For each adsorbate, the bars indicate the pH range where its surface coverage corresponds to a fraction of 10% or more, and the blue (red) color specifies a favorable (unfavorable) alignment between the band edges of semiconductor and the relevant redox levels. The vertical yellow stripe emphasizes near-neutral conditions with $5 \leq \mathrm{pH} \leq 9$.

similar to that of GaN but with a lower coverage of hydroxyl ions.

It is known that the photocatalytic efficiencies of pristine GaN and ZnO are still far from being satisfactory.[69,70] This is to a large extent due to their large band gaps ($> 3.2$ eV), which inhibit the efficient adsorption of solar light. Experimental observations indicate that alloying GaN with ZnO leads to a significant reduction of the band gap as the result of a slight downward shift of the conduction band edge and of a dramatically upward shift of the valence band edge.[71,72] For instance, it is sufficient to consider a $(GaN)_{1-x}(ZnO)_x$ alloy with $x$ as small as 0.13 to achieve a band gap decrease to 2.58 eV.[73] This is consistent with the GaN-ZnO alloy being a much more efficient photocatalyst than pristine GaN and ZnO, as demonstrated experimentally.[69,73–87] As for the alignment, there is sufficient margin to preserve the favorable band alignment upon alloying, since the valence band of GaN is found to be lower than the $OH^-/OH^\bullet$ level by as much as 1.25 eV (cf. Fig. 4). Our study provides additional insight shedding light on the surface coverage as a function of pH. From Fig. 5, it is reasonable to assume that in near-neutral conditions the ionic adsorbates would dominate on the surface of the GaN-ZnO alloy, as also observed in MD simulations carried out at the point of zero charge.[88] This leads to all metal sites and all non-metal sites at the surface being passivated by $OH^-$ and $H^+$ ions, respectively, constituting an ideal surface coverage for the overall water splitting (cf. Fig. 3). However, experimental results for the alloy $(GaN)_{0.87}(ZnO)_{0.13}$ indicate that it is necessary to add $RuO_2$ nanoparticles acting as co-catalyst to achieve overall water splitting, with the highest activity being obtained at pH $= 3$.[73] The co-catalyst is known to operate effectively in acidic conditions by promoting the hydrogen evolution reaction through the adsorption of protons.[89] Our results then suggests that the oxygen evolution reaction occurs through the $OH^-$ ions adsorbed on the Ga sites, since the Zn sites no longer present these ions in such acidic conditions (cf. Fig. 5). These considerations provide a rationale for designing GaN:ZnO alloys with a small content of ZnO.

As an alternative alloying strategy for GaN, the results in Fig. 5 suggest partial substitution of N with either As or P. In fact, the valence band edges of GaP and GaAs lie much

higher than that of GaN (cf. Fig. 4). Hence, a suitable concentration of P and As would also push up the valence band of the alloyed GaN and consequently reduce the band gap. Furthermore, despite the slightly different acidity at the N, P, and As sites, their $pK_a(H^+)$ values allow for a large fraction of protons to be adsorbed in near-neutral conditions (cf. Fig. 5).

The two polymorphs of $TiO_2$ also deserve attention, as they both show a favorable band alignment for hydrogen and oxygen evolutions. Nevertheless, their photocatalytic efficiency has remained low[90] and appears to be hindered, on the one hand, by the low concentration of adsorbed ionic species in near-neutral conditions (cf. Fig. 5) and, on the other hand, by the size of their band gaps ($> 3.0$ eV). Although active defect sites have been shown to promote water dissociation,[66,91,92] the amount of ionic adsorbates is apparently still insufficient to make the reaction viable at a satisfactory rate.[93,94] Compared to GaN and ZnO, the design of highly efficient catalysts based on $TiO_2$ for the overall water splitting reaction appears to be more complicated, as it would require not only a significant reduction of the band gap without deteriorating the good alignment of the energy levels, but also a substantial modification of the surface coverage. Nevertheless, N-doping has been extensively deployed for $TiO_2$ with the motivation of simultaneously narrowing the band gap and inducing a higher surface coverage of ionic species.[95–98] In an alternative approach, one could turn to nanoparticles of $TiO_2$ which possess smaller gaps and favor ionic adsorbates at their higher-energy surfaces.[99–106] Such surfaces have been demonstrated to be more reactive and to promote electron-transfer processes in dye-sensitized solar cells,[107] thus deserving a more in-depth investigation for water splitting.

# Conclusions

In this work, we present a theoretical formulation for investigating the pH-dependent surface coverage at semiconductor-water interfaces through the use of *ab initio* molecular dynamics

simulations and a grand-canonical formulation of adsorbates. Our study encompasses eight semiconductors, including GaAs, GaP, GaN, CdS, ZnO, $SnO_2$, rutile and anatase $TiO_2$. The present methodology allows us to calculate the acidity of individual adsorption sites at the interface, and consequently to derive the pH value at the point of zero charge ($pH_{PZC}$) as well as the fraction of dissociated water molecules at the surface. The calculated $pH_{PZC}$ show excellent agreement with their experimental counterparts, thereby supporting the validity of our formulation. Furthermore, based on the calculated $pK_a$ for the surface sites, we construct concentration diagrams of the interfacial adsorbates as a function of pH. By combining our results for the surface coverage and the band alignment, we investigate the potential of the considered semiconductors as photocatalysts for hydrogen and oxygen evolution and determine the corresponding pH ranges for optimal operation. Among the investigated semiconductors, our scheme naturally identifies GaN as the most promising candidate for the overall water splitting reaction and additionally indicates the possibility of achieving further improvement through alloying. The computational approach introduced in our work gives access to the characterization of materials properties that represent invaluable descriptors to identify optimal photocatalyst in the screening of materials. In particular, the site-specific acidic constants and the surface coverage remain at present beyond experimental reach.

## Conflicts of interest

There are no conflicts to declare.

## Acknowledgments

We acknowledge useful discussions with P. Gono. This work was performed in the context of the National Center of Competence in Research (NCCR) "Materials' Revolution: Computational Design and Discovery of Novel Materials (MARVEL)" of the Swiss National Science Foundation. This work was supported by a grant from the Swiss National Supercomputing

Center (CSCS) under project ID s879. We also used computational resources of EPFL at SCITAS and CSEA.

## Supporting Information

Section 1: Theoretical formulation for calculating acidity constants of semiconductor surface sites, pH-dependent surface coverage, and redox levels in solution and at semiconductor-water interfaces. Section 2: Description of semiconductor-water interfacial models and influence of adsorbates on surface structures. Section 3: Description of methods about how to run MD simulations, how to calculate deprotonation free energies and how to perform electrostatic finite-size and zero-point motion corrections. Section 4: Comparison of $\mathrm{pH_{PZC}}$ and $\mathrm{p}K_{\mathrm{a}}$ achieved at semilocal and hybrid levels. This material is available free of charge via the Internet at http://pubs.acs.org

## References

(1) Tachibana, Y.; Vayssieres, L.; Durrant, J. R. Artificial photosynthesis for solar water-splitting. *Nat. Photonics* **2012**, *6*, 511.

(2) Ahmad, H.; Kamarudin, S.; Minggu, L.; Kassim, M. Hydrogen from photo-catalytic water splitting process: A review. *Renewable Sustainable Energy Rev.* **2015**, *43*, 599–610.

(3) Kudo, A.; Miseki, Y. Heterogeneous photocatalyst materials for water splitting. *Chem. Soc. Rev.* **2009**, *38*, 253–278.

(4) Zou, X.; Zhang, Y. Noble metal-free hydrogen evolution catalysts for water splitting. *Chem. Soc. Rev.* **2015**, *44*, 5148–5180.

(5) Maeda, K.; Domen, K. Photocatalytic Water Splitting: Recent Progress and Future Challenges. *J. Phys. Chem. Lett.* **2010**, *1*, 2655–2661.

(6) Hisatomi, T.; Kubota, J.; Domen, K. Recent advances in semiconductors for photocatalytic and photoelectrochemical water splitting. *Chem. Soc. Rev.* **2014**, *43*, 7520–7535.

(7) Osterloh, F. E.; Parkinson, B. A. Recent developments in solar water-splitting photocatalysis. *MRS Bull.* **2011**, *36*, 17–22.

(8) Moniruddin, M.; Ilyassov, B.; Zhao, X.; Smith, E.; Serikov, T.; Ibrayev, N.; Asmatulu, R.; Nuraje, N. Recent progress on perovskite materials in photovoltaic and water splitting applications. *Mater. Today Energy* **2018**, *7*, 246–259.

(9) Walter, M. G.; Warren, E. L.; McKone, J. R.; Boettcher, S. W.; Mi, Q.; Santori, E. A.; Lewis, N. S. Solar Water Splitting Cells. *Chem. Rev.* **2010**, *110*, 6446–6473.

(10) Moniz, S. J.; Shevlin, S. A.; Martin, D. J.; Guo, Z.-X.; Tang, J. Visible-light driven heterojunction photocatalysts for water splitting–a critical review. *Energy Environ. Sci.* **2015**, *8*, 731–759.

(11) Fujishima, A.; Honda, K. Electrochemical photolysis of water at a semiconductor electrode. *Nature* **1972**, *238*, 37–38.

(12) Liu, J.; Liu, Y.; Liu, N.; Han, Y.; Zhang, X.; Huang, H.; Lifshitz, Y.; Lee, S.-T.; Zhong, J.; Kang, Z. Metal-free efficient photocatalyst for stable visible water splitting via a two-electron pathway. *Science* **2015**, *347*, 970–974.

(13) Luo, J.; Im, J.-H.; Mayer, M. T.; Schreier, M.; Nazeeruddin, M. K.; Park, N.-G.; Tilley, S. D.; Fan, H. J.; Grätzel, M. Water photolysis at 12.3% efficiency via perovskite photovoltaics and Earth-abundant catalysts. *Science* **2014**, *345*, 1593–1596.

(14) Khan, S. U. M.; Al-Shahry, M.; Ingler, W. B. Efficient Photochemical Water Splitting by a Chemically Modified n-$TiO_2$. *Science* **2002**, *297*, 2243–2245.

(15) Zou, Z.; Ye, J.; Sayama, K.; Arakawa, H. Direct splitting of water under visible light irradiation with an oxide semiconductor photocatalyst. *Nature* **2001**, *414*, 625.

(16) Kim, T. W.; Choi, K.-S. Nanoporous $BiVO_4$ photoanodes with dual-layer oxygen evolution catalysts for solar water splitting. *Science* **2014**, 1245026.

(17) Liao, L. et al. Efficient solar water-splitting using a nanocrystalline CoO photocatalyst. *Nature Nanotech.* **2014**, *9*, 69.

(18) Osterloh, F. E. Inorganic Materials as Catalysts for Photochemical Splitting of Water. *Chem. Mater.* **2008**, *20*, 35–54.

(19) Wu, Y.; Lazic, P.; Hautier, G.; Persson, K.; Ceder, G. First principles high throughput screening of oxynitrides for water-splitting photocatalysts. *Energy Environ. Sci.* **2013**, *6*, 157–168.

(20) Wu, Y.; Chan, M. K. Y.; Ceder, G. Prediction of semiconductor band edge positions in aqueous environments from first principles. *Phys. Rev. B* **2011**, *83*, 235301.

(21) Lin, Y.; Yuan, G.; Sheehan, S.; Zhou, S.; Wang, D. Hematite-based solar water splitting: challenges and opportunities. *Energy Environ. Sci.* **2011**, *4*, 4862–4869.

(22) Leng, W.; Barnes, P. R.; Juozapavicius, M.; O'Regan, B. C.; Durrant, J. R. Electron diffusion length in mesoporous nanocrystalline $TiO_2$ photoelectrodes during water oxidation. *J. Phys. Chem. Lett.* **2010**, *1*, 967–972.

(23) Li, X.; Dai, Y.; Li, M.; Wei, W.; Huang, B. Stable Si-based pentagonal monolayers: high carrier mobilities and applications in photocatalytic water splitting. *J. Mater. Chem. A* **2015**, *3*, 24055–24063.

(24) Scheuermann, A. G.; Lawrence, J. P.; Kemp, K. W.; Ito, T.; Walsh, A.; Chidsey, C. E.; Hurley, P. K.; McIntyre, P. C. Design principles for maximizing photovoltage in metal-oxide-protected water-splitting photoanodes. *Nat. Mater.* **2016**, *15*, 99.

(25) Ambrosio, F.; Wiktor, J.; Pasquarello, A. pH-Dependent Catalytic Reaction Pathway for Water Splitting at the $BiVO_4$-Water Interface from the Band Alignment. *ACS Energy Lett.* **2018**, *3*, 829–834.

(26) Ambrosio, F.; Wiktor, J.; Pasquarello, A. pH-Dependent Surface Chemistry from First Principles: Application to the $BiVO_4$(010)-Water Interface. *ACS Appl. Mater. Interfaces* **2018**, *10*, 10011–10021.

(27) Koper, M. T. Theory of multiple proton-electron transfer reactions and its implications for electrocatalysis. *Chem. Sci.* **2013**, *4*, 2710–2723.

(28) Guo, Z.; Ambrosio, F.; Chen, W.; Gono, P.; Pasquarello, A. Alignment of Redox Levels at Semiconductor-Water Interfaces. *Chem. Mater.* **2018**, *30*, 94–111.

(29) Gono, P.; Wiktor, J.; Ambrosio, F.; Pasquarello, A. Surface Polarons Reducing Overpotentials in the Oxygen Evolution Reaction. *ACS Catal.* **2018**, *8*, 5847–5851.

(30) Castelli, I. E.; Olsen, T.; Datta, S.; Landis, D. D.; Dahl, S.; Thygesen, K. S.; Jacobsen, K. W. Computational screening of perovskite metal oxides for optimal solar light capture. *Energy Environ. Sci.* **2012**, *5*, 5814–5819.

(31) Castelli, I. E.; Landis, D. D.; Thygesen, K. S.; Dahl, S.; Chorkendorff, I.; Jaramillo, T. F.; Jacobsen, K. W. New cubic perovskites for one- and two-photon water splitting using the computational materials repository. *Energy Environ. Sci.* **2012**, *5*, 9034–9043.

(32) Zhuang, H. L.; Hennig, R. G. Single-Layer Group-III Monochalcogenide Photocatalysts for Water Splitting. *Chem. Mater.* **2013**, *25*, 3232–3238.

(33) Katz, J. E.; Gingrich, T. R.; Santori, E. A.; Lewis, N. S. Combinatorial synthesis and high-throughput photopotential and photocurrent screening of mixed-metal oxides for photoelectrochemical water splitting. *Energy Environ. Sci.* **2009**, *2*, 103–112.

(34) Pham, T. A.; Ping, Y.; Galli, G. Modelling heterogeneous interfaces for solar water splitting. *Nat. Mater.* **2017**, *16*, 401.

(35) Gerosa, M.; Gygi, F.; Govoni, M.; Galli, G. The role of defects and excess surface charges at finite temperature for optimizing oxide photoabsorbers. *Nat. Mater.* **2018**, *17*, 1122.

(36) Ping, Y.; Rocca, D.; Galli, G. Electronic excitations in light absorbers for photoelectrochemical energy conversion: first principles calculations based on many body perturbation theory. *Chem. Soc. Rev.* **2013**, *42*, 2437–2469.

(37) Kharche, N.; Muckerman, J. T.; Hybertsen, M. S. First-principles approach to calculating energy level alignment at aqueous semiconductor interfaces. *Phys. Rev. Lett.* **2014**, *113*, 176802.

(38) Ertem, M. Z.; Kharche, N.; Batista, V. S.; Hybertsen, M. S.; Tully, J. C.; Muckerman, J. T. Photoinduced Water Oxidation at the Aqueous GaN $(10\bar{1}0)$ Interface: Deprotonation Kinetics of the First Proton-Coupled Electron-Transfer Step. *ACS Catal.* **2015**, *5*, 2317–2323.

(39) Zhang, C.; Hutter, J.; Sprik, M. Coupling of Surface Chemistry and Electric Double Layer at $TiO_2$ Electrochemical Interfaces. *J. Phys. Chem. Lett.* **2019**,

(40) Cheng, J.; Liu, X.; VandeVondele, J.; Sulpizi, M.; Sprik, M. Redox Potentials and Acidity Constants from Density Functional Theory Based Molecular Dynamics. *Acc. Chem. Res.* **2014**, *47*, 3522–3529.

(41) Cheng, J.; Liu, X.; Kattirtzi, J. A.; VandeVondele, J.; Sprik, M. Aligning Electronic and Protonic Energy Levels of Proton-Coupled Electron Transfer in Water Oxidation on Aqueous $TiO_2$. *Angew. Chem., Int. Ed.* **2014**, *126*, 12242–12246.

(42) Cheng, J.; Sprik, M. The electric double layer at a rutile $TiO_2$ water interface modelled using density functional theory based molecular dynamics simulation. *J. Phys.: Condens. Matter* **2014**, *26*, 244108.

(43) Li, Y.-F.; Selloni, A. Pathway of photocatalytic oxygen evolution on aqueous $TiO_2$ anatase and insights into the different activities of anatase and rutile. *ACS Catal.* **2016**, *6*, 4769–4774.

(44) Hörmann, N. G.; Guo, Z.; Ambrosio, F.; Andreussi, O.; Pasquarello, A.; Marzari, N. Absolute band alignment at semiconductor-water interfaces using explicit and implicit descriptions for liquid water. *npj Comput. Mater.* **2019**, *5*, 1–6.

(45) Chen, W.; Pasquarello, A. Band-edge positions in *GW*: Effects of starting point and self-consistency. *Phys. Rev. B* **2014**, *90*, 165133.

(46) Chen, W.; Pasquarello, A. Accurate band gaps of extended systems via efficient vertex corrections in *GW*. *Phys. Rev. B* **2015**, *92*, 041115.

(47) Xiao, H.; Tahir-Kheli, J.; Goddard, W. A. Accurate Band Gaps for Semiconductors from Density Functional Theory. *J. Phys. Chem. Lett.* **2011**, *2*, 212–217.

(48) Heyd, J.; Peralta, J. E.; Scuseria, G. E.; Martin, R. L. Energy band gaps and lattice parameters evaluated with the Heyd-Scuseria-Ernzerhof screened hybrid functional. *J. Chem. Phys.* **2005**, *123*, 174101.

(49) Tran, F.; Blaha, P. Accurate Band Gaps of Semiconductors and Insulators with a Semilocal Exchange-Correlation Potential. *Phys. Rev. Lett.* **2009**, *102*, 226401.

(50) Nørskov, J. K.; Rossmeisl, J.; Logadottir, A.; Lindqvist, L.; Kitchin, J. R.; Bligaard, T.; Jónsson, H. Origin of the Overpotential for Oxygen Reduction at a Fuel-Cell Cathode. *J. Phys. Chem. B* **2004**, *108*, 17886–17892.

(51) Valdés, Á.; Qu, Z.-W.; Kroes, G.-J.; Rossmeisl, J.; Nørskov, J. K. Oxidation and Photo-Oxidation of Water on $TiO_2$ Surface. *J. Phys. Chem. C* **2008**, *112*, 9872–9879.

(52) Li, Y.-F.; Liu, Z.-P.; Liu, L.; Gao, W. Mechanism and Activity of Photocatalytic Oxygen Evolution on Titania Anatase in Aqueous Surroundings. *J. Am. Chem. Soc.* **2010**, *132*, 13008–13015.

(53) Liao, P.; Keith, J. A.; Carter, E. A. Water Oxidation on Pure and Doped Hematite (0001) Surfaces: Prediction of Co and Ni as Effective Dopants for Electrocatalysis. *J. Am. Chem. Soc.* **2012**, *134*, 13296–13309.

(54) Cheng, J.; Sulpizi, M.; VandeVondele, J.; Sprik, M. Hole Localization and Thermochemistry of Oxidative Dehydrogenation of Aqueous Rutile $TiO_2$(110). *ChemCatChem* **2012**, *4*, 636–640.

(55) Todorova, M.; Neugebauer, J. Extending the Concept of Defect Chemistry from Semiconductor Physics to Electrochemistry. *Phys. Rev. Applied* **2014**, *1*, 014001.

(56) Ambrosio, F.; Miceli, G.; Pasquarello, A. Redox levels in aqueous solution: Effect of van der Waals interactions and hybrid functionals. *J. Chem. Phys.* **2015**, *143*, 244508.

(57) Vydrov, O. A.; Van Voorhis, T. Nonlocal van der Waals density functional: The simpler the better. *J. Chem. Phys.* **2010**, *133*, 244103.

(58) Sabatini, R.; Gorni, T.; de Gironcoli, S. Nonlocal van der Waals density functional made simple and efficient. *Phys. Rev. B* **2013**, *87*, 041108.

(59) Miceli, G.; de Gironcoli, S.; Pasquarello, A. Isobaric first-principles molecular dynamics of liquid water with nonlocal van der Waals interactions. *J. Chem. Phys.* **2015**, *142*, 034501.

(60) Ambrosio, F.; Miceli, G.; Pasquarello, A. Structural, Dynamical, and Electronic Properties of Liquid Water: A Hybrid Functional Study. *J. Phys. Chem. B* **2016**, *120*, 7456–7470.

(61) Cheng, J.; Sprik, M. Acidity of the Aqueous Rutile $TiO_2$(110) Surface from Density Functional Theory Based Molecular Dynamics. *J. Chem. Theory Comput.* **2010**, *6*, 880–889.

(62) Wang, Z.-T.; Wang, Y.-G.; Mu, R.; Yoon, Y.; Dahal, A.; Schenter, G. K.; Glezakou, V.-A.; Rousseau, R.; Lyubinetsky, I.; Dohnálek, Z. Probing equilibrium of molecular and deprotonated water on $TiO_2$(110). *Proc. Natl. Acad. Sci. U. S. A.* **2017**, *114*, 1801–1805.

(63) Zhang, X.; Ptasinska, S. Dissociative adsorption of water on an $H_2O$/GaAs(100) interface: in situ near-ambient pressure XPS studies. *J. Phys. Chem. C* **2014**, *118*, 4259–4266.

(64) Koike, K.; Yamamoto, K.; Ohara, S.; Kikitsu, T.; Ozasa, K.; Nakamura, S.; Sugiyama, M.; Nakano, Y.; Fujii, K. Effects of NiO-loading on n-type GaN photoanode for photoelectrochemical water splitting using different aqueous electrolytes. *Int. J. Hydrogen Energy* **2017**, *42*, 9493–9499.

(65) Maeda, K. Photocatalytic properties of rutile $TiO_2$ powder for overall water splitting. *Catal. Sci. Technol.* **2014**, *4*, 1949–1953.

(66) Schaub, R.; Thostrup, P.; Lopez, N.; Lægsgaard, E.; Stensgaard, I.; Nørskov, J. K.; Besenbacher, F. Oxygen Vacancies as Active Sites for Water Dissociation on Rutile $TiO_2$(110). *Phys. Rev. Lett.* **2001**, *87*, 266104.

(67) Ambrosio, F.; Guo, Z.; Pasquarello, A. Absolute Energy Levels of Liquid Water. *J. Phys. Chem. Lett.* **2018**, *9*, 3212–3216.

(68) Gono, P.; Ambrosio, F.; Pasquarello, A. Effect of the Solvent on the Oxygen Evolution Reaction at the $TiO_2$-Water Interface. *J. Phys. Chem. C* **2019**, *123*, 18467–18474.

(69) Yang, X.; Wolcott, A.; Wang, G.; Sobo, A.; Fitzmorris, R. C.; Qian, F.; Zhang, J. Z.; Li, Y. Nitrogen-doped ZnO nanowire arrays for photoelectrochemical water splitting. *Nano Lett.* **2009**, *9*, 2331–2336.

(70) Wang, D.; Pierre, A.; Kibria, M. G.; Cui, K.; Han, X.; Bevan, K. H.; Guo, H.; Paradis, S.; Hakima, A.-R.; Mi, Z. Wafer-Level Photocatalytic Water Splitting on GaN Nanowire Arrays Grown by Molecular Beam Epitaxy. *Nano Lett.* **2011**, *11*, 2353–2357.

(71) Di Valentin, C. Electronic Structure of $(Ga_{1-x}Zn_x)N_{1-x}O_x$ Photocatalyst for Water Splitting by Hybrid Hartree-Fock Density Functional Theory Methods. *J. Phys. Chem. C* **2010**, *114*, 7054–7062.

(72) Maeda, K.; Teramura, K.; Takata, T.; Hara, M.; Saito, N.; Toda, K.; Inoue, Y.; Kobayashi, H.; Domen, K. Overall Water Splitting on $(Ga_{1-x}Zn_x)(N_{1-x}O_x)$ Solid Solution Photocatalyst: Relationship between Physical Properties and Photocatalytic Activity. *J. Phys. Chem. B* **2005**, *109*, 20504–20510.

(73) Maeda, K.; Takata, T.; Hara, M.; Saito, N.; Inoue, Y.; Kobayashi, H.; Domen, K. GaN:ZnO Solid Solution as a Photocatalyst for Visible-Light-Driven Overall Water Splitting. *J. Am. Chem. Soc.* **2005**, *127*, 8286–8287.

(74) Arai, N.; Saito, N.; Nishiyama, H.; Inoue, Y.; Domen, K.; Sato, K. Overall water splitting by RuO2-dispersed divalent-ion-doped GaN photocatalysts with d10 electronic configuration. *Chem. Lett.* **2006**, *35*, 796–797.

(75) Maeda, K.; Teramura, K.; Lu, D.; Takata, T.; Saito, N.; Inoue, Y.; Domen, K. Photocatalyst releasing hydrogen from water. *Nature* **2006**, *440*, 295.

(76) Maeda, K.; Domen, K. Solid solution of GaN and ZnO as a stable photocatalyst for overall water splitting under visible light. *Chem. Mater.* **2009**, *22*, 612–623.

(77) Maeda, K.; Xiong, A.; Yoshinaga, T.; Ikeda, T.; Sakamoto, N.; Hisatomi, T.; Takashima, M.; Lu, D.; Kanehara, M.; Setoyama, T.; Teranishi, T.; Domen, K. Photocatalytic overall water splitting promoted by two different cocatalysts for hydrogen and oxygen evolution under visible light. *Angew. Chem., Int. Ed.* **2010**, *122*, 4190–4193.

(78) Ohno, T.; Bai, L.; Hisatomi, T.; Maeda, K.; Domen, K. Photocatalytic water splitting using modified GaN:ZnO solid solution under visible light: long-time operation and regeneration of activity. *J. Am. Chem. Soc.* **2012**, *134*, 8254–8259.

(79) Ren, B.; Zhang, X.; Zhao, M.; Wang, X.; Ye, J.; Wang, D. Significant enhancement in photocatalytic activity of $(GaN)_{1-x}(ZnO)_x$ nanowires via solubility and crystal facet tailoring. *AIP Adv.* **2018**, *8*, 015206.

(80) Shet, S.; Yan, Y.; Wang, H.; Ravindra, N.; Turner, J.; Al-Jassim, M. ZnO:GaN thin films for photoelectrochemical water splitting application. *Emerg. Mater. Res.* **2012**, *1*, 201–204.

(81) Sun, X.; Maeda, K.; Le Faucheur, M.; Teramura, K.; Domen, K. Preparation of $(Ga_{1-x}Zn_x)(N_{1-x}O_x)$ solid-solution from $ZnGa_2O_4$ and ZnO as a photo-catalyst for overall water splitting under visible light. *Appl. Catal. A: General* **2007**, *327*, 114–121.

(82) Maeda, K.; Teramura, K.; Saito, N.; Inoue, Y.; Domen, K. Improvement of photocatalytic activity of $(Ga_{1-x}Zn_x)(N_{1-x}O_x)$ solid solution for overall water splitting by co-loading Cr and another transition metal. *J. Catal.* **2006**, *243*, 303–308.

(83) Li, J.; Liu, B.; Yang, W.; Cho, Y.; Zhang, X.; Dierre, B.; Sekiguchi, T.; Wu, A.; Jiang, X. Solubility and crystallographic facet tailoring of $(GaN)_{1-x}(ZnO)_x$ pseudobi-

nary solid-solution nanostructures as promising photocatalysts. *Nanoscale* **2016**, *8*, 3694–3703.

(84) Edalati, K.; Uehiro, R.; Takechi, S.; Wang, Q.; Arita, M.; Watanabe, M.; Ishihara, T.; Horita, Z. Enhanced photocatalytic hydrogen production on GaN-ZnO oxynitride by introduction of strain-induced nitrogen vacancy complexes. *Acta Mater.* **2020**, *185*, 149–156.

(85) Abbas, Y.; Zuhra, Z.; Akhtar, N.; Ali, S.; Gong, J. Single-step fabrication of visible-light-active ZnO-GaN: ZnO branched nanowire array photoanodes for efficient water splitting. *ACS Appl. Energy Mater.* **2018**, *1*, 3529–3536.

(86) Wang, Z.; Han, J.; Li, Z.; Li, M.; Wang, H.; Zong, X.; Li, C. Moisture-Assisted Preparation of Compact GaN:ZnO Photoanode Toward Efficient Photoelectrochemical Water Oxidation. *Adv. Energy Mater.* **2016**, *6*, 1600864.

(87) Li, J.; Liu, B.; Wu, A.; Yang, B.; Yang, W.; Liu, F.; Zhang, X.; An, V.; Jiang, X. Composition and Band Gap Tailoring of Crystalline $(GaN)_{1-x}(ZnO)_x$ Solid solution nanowires for enhanced photoelectrochemical performance. *Inorg. Chem.* **2018**, *57*, 5240–5248.

(88) Kharche, N.; Hybertsen, M. S.; Muckerman, J. T. Computational investigation of structural and electronic properties of aqueous interfaces of GaN, ZnO, and a GaN/ZnO alloy. *Phys. Chem. Chem. Phys.* **2014**, *16*, 12057–12066.

(89) Sato, J.; Saito, N.; Yamada, Y.; Maeda, K.; Takata, T.; Kondo, J. N.; Hara, M.; Kobayashi, H.; Domen, K.; Inoue, Y. $RuO_2$-loaded $\beta$-$Ge_3N_4$ as a non-oxide photocatalyst for overall water splitting. *Journal of the American Chemical Society* **2005**, *127*, 4150–4151.

(90) Miyoshi, A.; Nishioka, S.; Maeda, K. Water Splitting on Rutile $TiO_2$-Based Photocatalysts. *Chem. Eur. J.* **2018**, *24*, 18204–18219.

(91) Walle, L.; Ragazzon, D.; Borg, A.; Uvdal, P.; Sandell, A. Competing water dissociation channels on rutile $TiO_2$(110). *Surf. Sci.* **2014**, *621*, 77–81.

(92) Aschauer, U.; He, Y.; Cheng, H.; Li, S.-C.; Diebold, U.; Selloni, A. Influence of Subsurface Defects on the Surface Reactivity of $TiO_2$: Water on Anatase (101). *J. Phys. Chem. C* **2010**, *114*, 1278–1284.

(93) Rhatigan, S.; Sokalu, E.; Nolan, M.; Colón, G. Surface Modification of Rutile $TiO_2$ with Alkaline-Earth Oxide Nanoclusters for Enhanced Oxygen Evolution. *ACS Appl. Nano Mater.* **2020**, *3*, 6017–6033.

(94) Ni, M.; Leung, M. K.; Leung, D. Y.; Sumathy, K. A review and recent developments in photocatalytic water-splitting using $TiO_2$ for hydrogen production. *Renewable and Sustainable Energy Rev.* **2007**, *11*, 401–425.

(95) Asahi, R.; Morikawa, T.; Ohwaki, T.; Aoki, K.; Taga, Y. Visible-light photocatalysis in nitrogen-doped titanium oxides. *Science* **2001**, *293*, 269–271.

(96) Zhao, Z.; Li, Z.; Zou, Z. Water Adsorption and Decomposition on N/V-Doped Anatase $TiO_2$(101) Surfaces. *J. Phys. Chem. C* **2013**, *117*, 6172–6184.

(97) Morikawa, T.; Asahi, R.; Ohwaki, T.; Aoki, K.; Taga, Y. Band-Gap Narrowing of Titanium Dioxide by Nitrogen Doping. *Jpn. J. Appl. Phys.* **2001**, *40*, L561.

(98) Wang, C.; Hu, Q.; Huang, J.; Wu, L.; Deng, Z.; Liu, Z.; Liu, Y.; Cao, Y. Efficient hydrogen production by photocatalytic water splitting using N-doped $TiO_2$ film. *Appl. Surf. Sci.* **2013**, *283*, 188–192.

(99) Yang, H. G.; Sun, C. H.; Qiao, S. Z.; Zou, J.; Liu, G.; Smith, S. C.; Cheng, H. M.; Lu, G. Q. Anatase $TiO_2$ single crystals with a large percentage of reactive facets. *Nature* **2008**, *453*, 638.

(100) Wu, B.; Guo, C.; Zheng, N.; Xie, Z.; Stucky, G. D. Nonaqueous Production of Nanostructured Anatase with High-Energy Facets. *J. Am. Chem. Soc.* **2008**, *130*, 17563–17567.

(101) Han, X.; Kuang, Q.; Jin, M.; Xie, Z.; Zheng, L. Synthesis of titania nanosheets with a high percentage of exposed (001) facets and related photocatalytic properties. *J. Am. Chem. Soc.* **2009**, *131*, 3152–3153.

(102) Ma, X. Y.; Chen, Z. G.; Hartono, S. B.; Jiang, H. B.; Zou, J.; Qiao, S. Z.; Yang, H. G. Fabrication of uniform anatase $TiO_2$ particles exposed by {001} facets. *Chem. Commun.* **2010**, *46*, 6608–6610.

(103) Li, J.; Xu, D. Tetragonal faceted-nanorods of anatase $TiO_2$ single crystals with a large percentage of active {100} facets. *Chem. Commun.* **2010**, *46*, 2301–2303.

(104) Wen, C. Z.; Zhou, J. Z.; Jiang, H. B.; Hu, Q. H.; Qiao, S. Z.; Yang, H. G. Synthesis of micro-sized titanium dioxide nanosheets wholly exposed with high-energy {001} and {100} facets. *Chem. Commun.* **2011**, *47*, 4400–4402.

(105) Zhao, X.; Jin, W.; Cai, J.; Ye, J.; Li, Z.; Ma, Y.; Xie, J.; Qi, L. Shape-and size-controlled synthesis of uniform anatase $TiO_2$ nanocuboids enclosed by active {100} and {001} facets. *Adv. Funct. Mater.* **2011**, *21*, 3554–3563.

(106) Wen, C. Z.; Jiang, H. B.; Qiao, S. Z.; Yang, H. G.; Lu, G. Q. M. Synthesis of high-reactive facets dominated anatase $TiO_2$. *J. Mater. Chem.* **2011**, *21*, 7052–7061.

(107) Martsinovich, N.; Troisi, A. How $TiO_2$ crystallographic surfaces influence charge injection rates from a chemisorbed dye sensitiser. *Phys. Chem. Chem. Phys.* **2012**, *14*, 13392–13401.

# Graphical TOC Entry